Reviewer #1

This manuscript presents an advancement in droplet freezing techniques (DFTs) for measuring ice-nucleating particles (INPs) via immersion freezing. The development of FINDA-WLU addresses uncertainties in temperature control, detection accuracy, and operational efficiency. While the study is methodologically sound and provides validation data, several aspects require clarification to establish the novelty and reliability of the instrument. Below are detailed comments and suggestions for improvement.

We would like to thank the reviewers for their thoughtful comments that helped improve our manuscript. We revised the manuscript accordingly and think it has strengthened as a result. Please find our point-by-point response in blue text. Additions to the text are shown in *italics with an underline*. All line numbers refer to the new version of the manuscript. A tracked changes version is also included.

The authors claim improvements in hardware, software, and temperature calibration, but the specific innovations need explicit articulation. Compared to prior FINDA designs, FINDA-WLU achieves ±0.60°C uncertainty. However, the manuscript should clarify how the heat transfer efficiency (vertical) and temperature homogeneity (horizontal) were optimized.

Thank you for your suggestions. Compared to the original version of FINDA (Ren et al., 2024), the FINDA-WLU has undergone structural optimization, ensuring a more secure fixation of components such as the CCD and LED lights. Most importantly, the design of the core element, the aluminum block cold stage, has been re-engineered to enhance both performance and stability. In the previous version, four Pt100 sensors were attached to the inner bottom of the four corner wells of the 96-well plate, and these wells were then fixed to the cold stage. In FINDA-WLU, the wells designed to accommodate the four Pt100 sensors have been repositioned to the outer edge of the 96-well plate, eliminating the need to cut the four corners of the PCR plate before each experiment.

Regarding the software, the original version of FINDA used three separate software packages to control the chiller, read the Pt100 data, and acquire the CCD image. In contrast, FINDA-WLU combines all these functions into a single software package. The updated software in FINDA-WLU also includes automated grayscale analysis and calculation of INP number concentrations. We added the following text in Lines 140 to 144:

"The program can analyze the temporal resolution of grayscale values and determine the frozen temperature of each droplet (details in Sect. 2.3). The frozen fraction and INP number concentration (for both water and air filter samples) are then calculated based on input sample information (calculation methods in Sect. 4.5)."

Regarding temperature homogeneity, FINDA-WLU includes single-well temperature calibration, as explained in Sect. 2.4.4, Horizontal Temperature Calibration.

Since the original version of FINDA was only briefly introduced in the INP measurements of hailstones in China in Ren et al. (2024), which is not an instrumentation article, we did not provide

a detailed comparison of the original FINDA and FINDA-WLU in our manuscript. We referenced the original version of FINDA in the introduction: "*In this study, we present the newly developed Freezing Ice Nucleation Detector Array at Westlake University (FINDA-WLU), building on the original version of FINDA briefly introduced in Ren et al. (2024).*"

While "user-friendly software" is mentioned, details on real-time monitoring, automated droplet tracking, or data processing algorithms are lacking.

The real-time monitoring is mentioned in Lines 130-132:" *A customized National Instruments LabVIEW program was developed to control the experiment via a user interface panel shown in Fig. 2, including controlling the coolant bath circulator and monitoring the freezing status of droplets in the PCR plate with a CCD camera.*"

We added the following information in Sect. 2.2, Software control.

"*The program can analyze the temporal resolution of grayscale values and determine the frozen temperature of each droplet (details in Sect. 2.3). The frozen fraction and INP number concentration (for both water and air filter samples) are then calculated based on input sample information (calculation methods in Sect. 4.5).*"

The study asserts high precision but omits comparisons with other DFTs (e.g., number of droplets processed per run, false-positive rates). It is recommended to contrast FINDA-WLU directly with existing DFTs in a table, highlighting metrics like droplet capacity, temperature resolution, and uncertainty.

Thank you for your valuable suggestions. We concur with your view that a table summarizing the current DFTs would indeed be very beneficial for readers. However, it is important to note that Miller et al. (2021) have already provided such a table, specifically Table 1.

To address your concern, we have organized a new table based on the one from Miller et al. (2021), which incorporated additional information—such as temperature cooling rate, temperature uncertainty, and T_{50} of water background. Nevertheless, given that Miller et al. (2021) have already presented the majority of the information, we have chosen not to include this table in the manuscript unless the reviewers strongly recommend otherwise.

Table 1. Comparison of droplet freezing techniques (DFTs).

Name	Description	Drop Size	Drops	T range (°C)	Cooling rate (K min-1)	T uncertainty (°C)	T_{50} of MilliQ (°C)	Citation
	combining microfluidic droplet generation and collection with a Peltier-based cold stage	83-99 µm; 2 µL add 2 µL oil	250-500	to −45 (Peltier)	1-10	0.5		Tarn et al., 2018

CMU-CS	the Carnegie Mellon University Cold Stage system	~ 0.1 µL	30-40	10 to −40	1	0.5		Polen et al., 2016
FDF	the combined membrane filter-drop freezing technique	1±0.1 µL	~ 40, maximum 130	to ~ −30	1	0.4 (µL-NIPI)	~ −27.5; ~ −30	Price et al., 2018; Schnell, 1982
µL-NIPI	the microlitre Nucleation by Immersed Particle Instrument	1±0.025 µL	~ 40	1 to −35	1	0.4	~ −26	Whale et al., 2015
BINARY	the Bielefeld Ice Nucleation ARraY	1 µL (0.5-5 µL)	36	5 to −40	1 (could be 0.1-10)	0.3		Budke and Koop, 2015
WACIFE	a Grant-Asymptote EF600 cold stage	1.0±0.1 µL, 60-129 µm	~ 33	to −40	1, 10	0.4	~ −26	Wilson et al., 2015
PKU-INA	PeKing University Ice Nucleation Array	1 µL	90	0 to −30	0.1-10	0.4	~ −28	Chen et al., 2018
LINA	Leipzig Ice Nucleation Array	1 µL	90	5 to −40 (same to BINARY)	1	0.5	~ −30	Chen et al., 2018
	a pyroelectric thermal sensor	1 µL		to −30	1	0.8		Cook et al., 2020
FRIDGE-TAU	FRankfurt Ice-nuclei Deposition freezinG Experiment, the Tel Aviv University version	2 µL	100-130	−18 to −27	1		−24	Ardon-Dryer et al., 2011
DFCP	the NOAA drop freezing cold plate	2.5 µL	100	to −33	1-10	0.2	~ −30	Baustian et al., 2010;
TINA	the Twin-plate Ice Nucleation Assay	3 µL (0.1-40 µL)	192, 768	−1.5 to −40.15	1-10	0.2	~ −26	Kunert et al., 2018
	a cold stage in single crystals	3 µL		10 to −30	3			Mignani et al., 2019
CRAFT	the Cryogenic Refrigerator Applied to Freezing Test	5 µL	49	50 to −80	1	0.2	~ −35	Tobo et al., 2016
FINC	Freezing Ice Nuclei Counter	5-60 µL	288	to −30	1	0.5	−25.2 (50µL)	Miller et al., 2021
	flow cell microscopy	20-22 µL		to −43.15, −93.15 (230 K, 180 K)	5	0.1		Koop et al., 2000
AIS	the Automated Ice Spectrometer	50 µL	192	15 to −33	0.69-0.87	horizontal 0.3; vertical 0.6		Beall et al., 2017

INSEKT	the Ice Nucleation SpEctrometer of the Karlsruhe Institute of Technology	50 µL	32 (192 in total)	0 to −25.15 (248 K to 268 K)	0.33	0.3		Schiebel, 2017(thesis)
IR-NIPI	the InfraRed-Nucleation by Immersed Particles Instrument	50 µL	96	to −90	1	0.9	~ −18 to −23	Harrison, et al., 2018
INDA	Ice Nucleation Droplet Array	50 µL	96	to −30	1	0.5	~ −14 to −16	Chen et al., 2018
DRINCZ	the DRoplet Ice Nuclei Counter Zurich	50 µL	96	0 to −30	1	0.9 (reproducible 0.3; horizontal 0.6)	~ −22.5	David et al., 2019
DFT	the droplet freezing technique	50 µL	48	0 to −30	0.67	1	~ −23	Gute and Abbatt, 2020
CSU-IS	CSU Ice Spectrometer	50 µL	32	to −30	0.33		start −25	Barry et al., 2021
	drop freezing apparatus for filters	0.1 mL	108	to −12	0.33 (record frozen per 1 °C)			Conen et al., 2012
	a high throughput screening platform involving microplates	150 µL	96-768	2 to −25	0.2			Zaragotas et al., 2016
LINDA	LED-based Ice Nucleation Detection Apparatus	200 µL (40-400 µL)	52	to −15	0.4	0.2 (repeated)		Stopelli et al., 2014
MINA	the mono ice nucleation assay		(PCR)	−5 to −15	2 for 12 min			Pummer et al., 2015
MOUDI −DFT	the micro-orifice uniform deposit impactor-droplet freezing technique (Chow and Watson, 2007)	0.056-18 µm		to −40	to −40	0.3		Mason et al., 2015
	droplet freezing technique	1-40 µm	200−800	−15.15 to −30.15	0.1			Dymarska et al., 2006
	flow cell microscopy technique for aerosol phase transitions	7-33µm	65	to −103.15	2−12	1 (0.1 at 0 °C)		Salcedo et al., 2000
Leeds−NIPI	Nucleation by Immersed Particle Instrument	10^{-12} to 10^{-6} L (8 µm to 1.45 mm)		−6 to −36	10	0.4		O'Sullivan et al., 2014

		10-40 μm	10−230	to −45.15 (228 K)	2.5−10	0.6	−32.35	Murray et al., 2010; Murray et al., 2011
		10-200 μm		~ 15.15 to −39.15	1−2	The Peltier element below 220K, <1	~ −36.15	Pummer et al., 2012
	a freezing chip	20-80 μm, 4-300 pL	~25	to −40	2	0.4	−37.5	Häusler et al.. 2018
	an FDCS196 cryostage	~ 35 μm	~200	to −40	1	0.1 (for TMS 94)	−9	Weng et al., 2017
WISDOM	The WeIzmann Supercooled Droplets Observation on Microarray	40, 100 μm	500, 120	13.15 to −38.15 (260 K to 235 K)	0.1−10	1		Reicher et al., 2018
	(Wright and Petters, 2013; Bigg, 1953)	50-300 μm	~100−500	−4 to −33	5	1		Wright et al., 2013
	the differential scanning calorimeter (DSC) measurements, and the cryo-microscope experiments	~53-96 μm	a few thousand	to −50	1 (from −10°C to lower temperature)	0.3		Riechers et al., 2013
	combining microfluidic droplet generation and collection with a Peltier−based cold stage	83-99 μm; 2 μL add 2 μL oil	250−500	to −45 (Peltier)	1−10	0.5		Tarn et al., 2018
SBM	soccer ball model (Niedermeier, 2011, 2014, 2015)	215±70 pL, 107±14 μm	1200−1500+	126.85 to −196.15	0.01−100	0.1 (from −40°C to 30°C)		Peckhaus et al., 2016
	a “store and create” microfluidic device	6 nL (5.8±0.7 nL) equal to 300±18 μm	720	0 to −33	1	0.2	−33.7±0.4	Brubaker et al., 2020

Fig. 7 reveals horizontal temperature gradients on the cold stage. While common in DFTs, this issue significantly impacts INP quantification, as ±0.6°C uncertainty may affect INP concentrations to a large extent. How do these gradients affect the freezing temperature statistics (e.g., broadening of spectra)? The original FINDA used dynamic infrared imaging for calibration; FINDA-WLU's "rigorous temperature calibrations" and final INP concentration calibration require elaboration (e.g., correction algorithms).

To obtain the temperature calibration, we compare the frozen fraction curve after the single-well temperature calibration with that before the calibration for pure water and Snomax samples, as shown in Fig. C1.

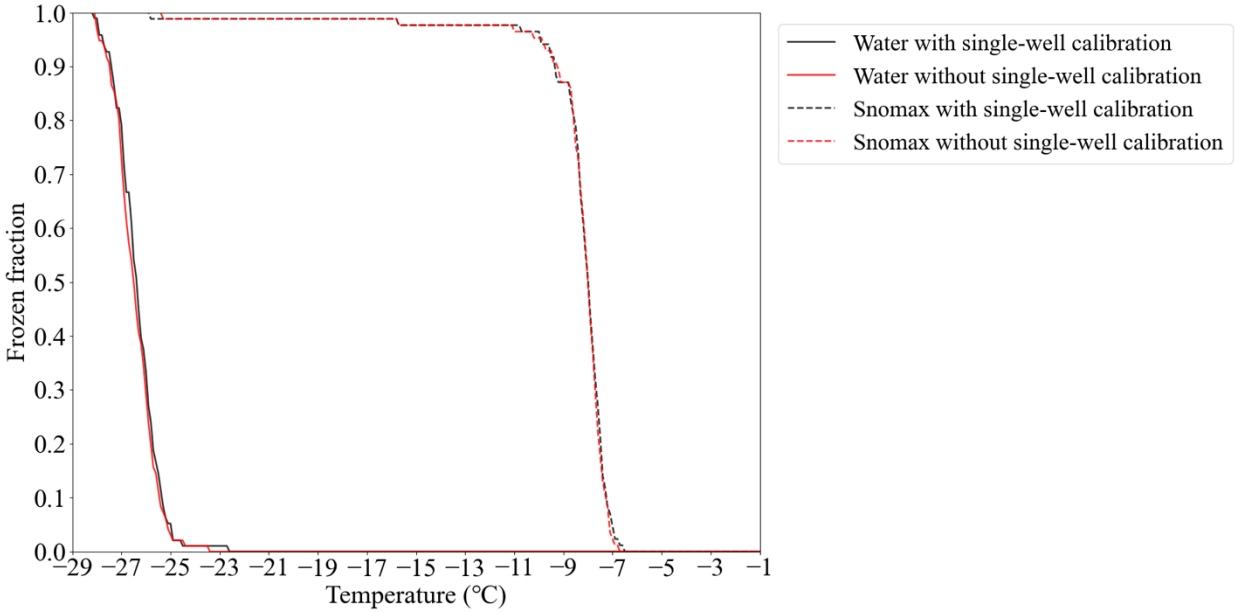

Fig C1. Frozen fraction curve of Milli-Q water with and without single-well temperature calibration in solid black and red lines, respectively. Frozen fraction of Snomax sample with and without single-well temperature calibration in dashed black and red lines, respectively.

Actually, the FF difference between with and without single-well calibration is not significant, even lower than the FF uncertainties (method in Sect. 3 INP concentration calibration). As the chiller itself causes the horizontal temperature gradients, we strongly recommend that the DFTs include the single-well temperature calibration.

The correction algorithms were already provided in the original manuscript in Lines 257 to 263 (now Lines 259 to 265).

"To address the horizontal temperature heterogeneity of the PCR plate, an individual-well calibration approach was conducted. The mean temperature of the four calibrated Pt100 sensors (T_{C_mean}) was used to calibrate the temperature of each PCR well:

$$T_{C\_Infrared_i} = a_i \times T_{C\_mean} + b_i \quad (i = 1, 2, 3, \ldots, 96), \qquad (3)$$

where $T_{C\_Infrared_i}$ is the calibrated temperature of the i^{th} well, and a_i and b_i are the slope and intercept of the regression, respectively. For each PCR well, a standard deviation of Eq. (3) is calculated, and two times the largest standard deviation (±0.22 °C) is treated as the uncertainty for this step."

Fig. 8 shows Milli-Q water freezing at −22°C to −24°C, differing from the listed literature (−13, −14°C). It should specify droplet volumes (not mentioned) and compare with previous studies. It is recommended to test water with documented ultrapure standards and add comparisons to ≥3 DFT studies, especially for studies using similar droplet volumes and numbers, and temperature ranges.

We already had included the information on the droplet size in the manuscript. In the original version of the manuscript, we stated:" *It is worth noting that the droplets measured by micro-PINGUIN (30 µL) and DRINCZ (50 µL) are smaller than or equal to that (50 µL) used in this study.*"

In the revised version of the manuscript, we include more information about different DFTs for the comparison.

"It is worth noting that the droplet sizes examined in FINC (5 µL) and Micro-PINGUIN (30 µL) are smaller than in FINDA-WLU, while the droplet size used in other DFTs, such as DRINCZ, is equal to the one in FINDA-WLU."

Also, we now compare water background measurements of more DFT studies, including FINC (Miller et al., 2021), Micro-PINGUIN (Wieber et al., 2024), DRINCZ (David et al., 2019), IR-NIPI (Harrison et al., 2018), and INDA (Chen et al., 2018) to our data (see Figure 8). In particular, the droplet sizes measured by different studies are indicated in the updated Figure (Figure 8).

Below is the updated Figure 8. Our Milli-Q water background (denoted by solid lines) is still one of the lowest among the above-mentioned studies. We changed the main text accordingly.

"The FF of Milli-Q water droplets using DFTs with different volumes, including Freezing Ice Nuclei Counter (FINC) (Miller et al., 2021), microtiter plate-based ice nucleation detection results in gallium (Micro-PINGUIN) (Wieber et al., 2024), Droplet Ice Nuclei Counter Zurich (DRINCZ) (David et al., 2019), InfraRed-Nucleation by Immersed Particles Instrument (IR-NIPI) (Harrison et al., 2018), and Ice Nucleation Droplet Array (INDA) (Chen et al., 2018), are shown in Fig. 8 for comparison. In general, FINDA-WLU (T_{50} = –26.5 ± 0.04 ℃) shows a considerably lower T_{50} compared to those measured by INDA (T_{50} = –25.5 ℃), FINC (T_{50} = –25.4 ℃), DRINCZ (T_{50} = –22.2 ℃), IR-NIPI (T_{50} = –21.0 ℃), and Micro-PINGUIN (T_{50} = –20.8 ℃)."

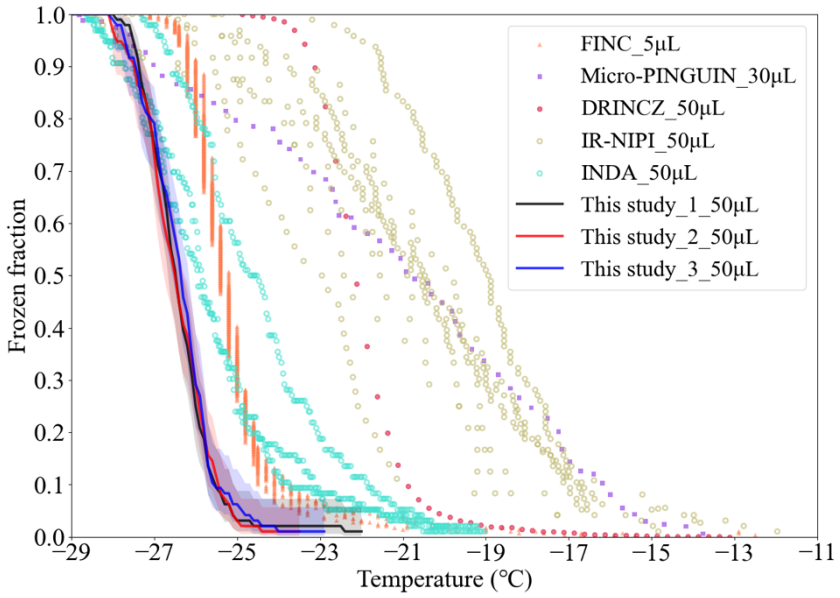

"*Figure 8: Frozen fraction of Milli-Q water. The results of FINDA-WLU are shown as solid lines. The shaded area indicate the measurement uncertainties. Results for other droplet freezing techniques, including FINC (Miller et al., 2021), Micro-PINGUIN (Wieber et al., 2024), DRINCZ (David et al., 2019), IR-NIPI (Harrison et al., 2018), and INDA (Chen et al., 2018), are shown as triangles, squares, dots, and circles, respectively.*"

High-concentration dust suspensions (e.g., −2°C onset) in Fig. 9 likely do not reflect atmospheric conditions (typical INP onset: <−15°C). In high concentration suspensions, multiple INPs compete, altering freezing kinetics. Which curves are similar to real atmospheric conditions? Precipitation samples are mentioned but not linked to dust or biological results. Do these samples exhibit similar freezing behavior?

We agree that the high-concentration dust suspensions (e.g., −2°C onset) in Fig. 9 does not reflect the particle concentration in a cloud droplet under atmospheric-relevant conditions. The use of different suspension concentrations is to validate the performance of the FINDA-WLU over a broader temperature range, as droplets with higher particle concentration tend to freeze at a higher temperature. The ability of DFTs to capture ice nucleation events at higher temperatures is important to quantify INP species that are highly ice efficient but exist at low concentrations in the atmosphere.

Regarding atmospheric relevance, it is worth noting that Fig. 9 provides n_m data, which normalizes the freezing ability of the examined sample by particle mass, making n_m independent of particle mass concentrations in single droplets. When applying the conversion by Vali (1971) and to obtain INP concentrations, the assumption of a Poisson distribution of INPs in the droplets is made. This corrects for multiple INPs in single droplets. Overall, n_m is atmospherically revelant and it can estimate the INP number produced by dust particles as long as the particle mass is known. This, as you say, is only true as long as competition for water does not play a role. However, given the comparably large water volume in the examined droplets, we assume that such a competiton does not occur.

A bump at the temperature above −20 °C indicates a contribution of bioaerosol, as observed in our precipitation samples (Fig. 11). This aligns with the findings from many other previous studies (Conen et al., 2011). However, to verify the presence of biological or dust INPs and quantify their contributions, further experiments such as chemical and biological characterizations and heating treatments of samples are needed. As we do not have leftovers of our precipitation samples to do more experiments, and the source characterization of these precipitation samples is not the purpose of this study, no further discussion is added to the original manuscript.

In the manuscript, we stated "*The high INP concentrations in cloud water, snow, and hail at warm temperatures (>–18.0 °C) suggest that biological aerosols might make a great contribution to INPs. Further chemical analysis and heating treatments of samples will help in the future to confirm the nature and sources of INPs.*"

It is recommended to include error bars in INP spectra, e.g., Figs. 8–9, to reflect uncertainty.

We totally agree that the error bars (more precisely, the uncertainties) should be included in the results, and we have included the uncertainties in this study, as indicated by error bars in Figs. 8

and 9. But previous studies are lacking this information, which is why we don't have error bars for previous studies in the Figs. 8 and 9.

Reference:

Chen, J., Wu, Z., Augustin-Bauditz, S., Grawe, S., Hartmann, M., Pei, X., Liu, Z., Ji, D., and Wex, H.: Ice-nucleating particle concentrations unaffected by urban air pollution in Beijing, China, Atmospheric Chemistry and Physics, 18, 3523-3539, 10.5194/acp-18-3523-2018, 2018.

Conen, F., Morris, C. E., Leifeld, J., Yakutin, M. V., and Alewell, C.: Biological residues define the ice nucleation properties of soil dust, Atmos. Chem. Phys., 11, 9643-9648, 10.5194/acp-11-9643-2011, 2011.

David, R. O., Cascajo-Castresana, M., Brennan, K. P., Rösch, M., Els, N., Werz, J., Weichlinger, V., Boynton, L. S., Bogler, S., Borduas-Dedekind, N., Marcolli, C., and Kanji, Z. A.: Development of the DRoplet Ice Nuclei Counter Zurich (DRINCZ): validation and application to field-collected snow samples, Atmos. Meas. Tech., 12, 6865-6888, 10.5194/amt-12-6865-2019, 2019.

Harrison, A. D., Whale, T. F., Rutledge, R., Lamb, S., Tarn, M. D., Porter, G. C. E., Adams, M. P., McQuaid, J. B., Morris, G. J., and Murray, B. J.: An instrument for quantifying heterogeneous ice nucleation in multiwell plates using infrared emissions to detect freezing, Atmospheric Measurement Techniques, 11, 5629-5641, 10.5194/amt-11-5629-2018, 2018.

Miller, A. J., Brennan, K. P., Mignani, C., Wieder, J., David, R. O., and Borduas-Dedekind, N.: Development of the drop Freezing Ice Nuclei Counter (FINC), intercomparison of droplet freezing techniques, and use of soluble lignin as an atmospheric ice nucleation standard, Atmos. Meas. Tech., 14, 3131-3151, 10.5194/amt-14-3131-2021, 2021.

Ren, Y., Fu, S., Bi, K., Zhang, H., Lin, X., Cao, K., Zhang, Q., and Xue, H.: Freezing Nucleus Spectra for Hailstone Samples in China From Droplet Freezing Experiments, Journal of Geophysical Research: Atmospheres, 129, e2023JD040505, 10.1029/2023JD040505, 2024.

Vali, G.: Quantitative evaluation of experimental results an the heterogeneous freezing nucleation of supercooled liquids, Journal of Atmospheric Sciences, 28, 402-409, 1971.

Wieber, C., Rosenhøj Jeppesen, M., Finster, K., Melvad, C., and Šantl-Temkiv, T.: Micro-PINGUIN: microtiter-plate-based instrument for ice nucleation detection in gallium with an infrared camera, Atmos. Meas. Tech., 17, 2707-2719, 10.5194/amt-17-2707-2024, 2024.